Estimation of diurnal hydraulic status of spruce trees using drone-based hyperspectral images and green shoulder indices

Chiara Zabeo[1], Luiz Henrique Elias Cosimo[1], Leonie Schönbeck[2], Jose Gutierrez Lopez[3], Langning Huo[1]

[1] Department of Forest Resource Management, SLU, Skogsmarksgränd Umeå, Sweden – chiara.zabeo@slu.se, luiz.cosimo@slu.se, langning.huo@slu.se,

[2] Southern Swedish Forest Research Centre, SLU, Sundsvägen 3 Alnarp, Sweden - leonie.schonbeck@slu.se

[3] Department of Forest Ecology and Management, SLU, Skogsmarksgränd Umeå, Sweden – jose.lopez@slu.se

Keywords: UAV, hyperspectral imagery, spectral indices, sap flux, water potential, boreal forests

Abstract

Tree hydraulic status fluctuates throughout the day as solar radiation and vapor pressure deficit (VPD) regulate transpiration and stomatal conductance. Remote Sensing (RS) can capture these dynamics, particularly through optical wavelengths in the “green shoulder” region (490–550 nm), which are sensitive to physiological changes in vegetation. This study evaluates the performance of the commonly employed Photochemical Reflectance Index (PRI) and four Green Shoulder Curvature Ratio (GSCR) indices derived from hyperspectral imagery as indicators of hydraulic status and photosynthetic efficiency in Norway spruce. Data were collected in the Tönnersjöheden experimental forest in southern Sweden. Four hyperspectral Unmanned Aerial Vehicles (UAV) flights were conducted throughout the same day on two occasions: Week 33 (mid-August) and Week 39 (late September) of 2025. Spectral indices were compared with sap flux density (Js) measurements (Week 33) through logistic regression leaf water potential (Ψ_{leaf}) data (Week 39) through linear models. Daily Green Shoulder Indices (GSI) time series were further compared with Photosynthetically Active Radiation (PAR) daily trajectories using the approximate area between curves. GSCR indices consistently outperformed PRI in following diurnal hydraulic status based on Js, while relationships with Ψ_{leaf} were mainly insignificant, likely due to the limited number of measurements available and less precise time pairing with UAV imagery. However, linear regression of the Ψ_{leaf}-GSI datasets followed similar trajectories as the Js-GSI relationships. GSCR indices generally tracked PAR trajectories more closely than PRI; however, results were mainly inconsistent between the two weeks, suggesting a lack of generalizability.

1. Introduction

The estimation of tree hydraulic status is a complex phenomenon involving interaction between various factors, whether environmental, such as climatic conditions and soil properties, or genetic, involving differences among individual plants. Since the investigation of tree hydraulic status depends on sensors measuring single trees, Remote Sensing (RS) methods are used to assess and widen the extent of the analysis over larger areas, from stand to landscape level. When it comes to optical RS data, integration within tree hydraulic status monitoring framework is possible based on the fact that certain wavelengths in the electromagnetic spectrum are sensitive to plant water content or to physiological changes in the canopy associated with water dynamics and allow to assess its status at a definite moment in time or monitor its change when a time series is available.

Among the wavelengths that are sensitive to modifications in tree water content there is the so-called “green shoulder”, a portion of the spectrum between blue and green wavelengths (490–550 nm) that has been shown to be directly connected to photosynthetic activity and Light Use Efficiency (LUE; Huo et al., 2024); the connection to hydraulic status estimation is given by the fact that photosynthesis downregulation is initiated through drought-induced stomatal closure, thus reducing atmospheric CO_2 uptake. This decreases the amount of light needed to saturate photosynthesis, creating an excess of energy to be dissipated (D’Odorico et al., 2021). The xanthophyll cycle represents an adaptive strategy for excess energy dissipation throughout the day, involving the conversion of violaxanthin to zeaxanthin as temperatures increase (Demmig-Adams & Adams, 1996; Niyogi, 1999).

Among the Green Shoulder Indices (GSI), which are vegetation indices (VIs) formulated using specific wavelengths from the green shoulder region, the Photochemical Reflectance Index (PRI, Gamon et al., 1997) is widely used to assess tree ecophysiological mechanisms due to its link with photosynthetic activity. In fact, PRI has been used to study photosynthetic response in crops (Gitelson et al., 2017; Inoue & Peñuelas, 2006; Lin et al., 2026) and in *Pinus sylvestris* L. stands in boreal forests (Möttus et al., 2018) or to study drought stress in pine stands under controlled drought experimental design (D’Odorico et al., 2021); however, studies in natural forest ecosystems involving collection of high-resolution hyperspectral images throughout the same day to assess daily cycle of tree hydraulic status are still lacking and few records, such as that by D’Odorico et al. (2021), of similar study designs are available.

Previous studies highlight the limitations connected to PRI, such as its tendency to be influenced by soil background (Gitelson et al., 2017), canopy structure, pigment pools or changing solar-viewing angles (D’Odorico et al., 2021; Lin et al., 2026) which make it unsuitable to track daily LUE dynamics under certain conditions. To address the limitations presented by PRI, Huo et al. (2024) developed Green Shoulder Curvature Ratio (GSCR) indices based on the observation that the peak and valley values of the first and second derivative curves in the green shoulder region are consistently related to shifts in photosynthetic capacity. GSCR indices have already been proven by Huo et al. (2024) to be suitable to detect reduction of photosynthetic

https://doi.org/10.5194/isprs-archives-XLIX-B3-2026-1171-2026

capacity in trees affected by the European spruce bark beetle (*Ips typographus* L.).

This study aims to assess the performance of GSIs across high spatial, spectral, and temporal resolutions, while also addressing the need for further evaluation of GSCR indices in relation to tree ecophysiology. These motivations are the drivers behind this study, where We monitor the suitability of the GSCR indices to track tree hydraulic status and follow Photosynthetically Active Radiation (PAR) daily trajectory in a Norway spruce (*Picea abies* (L.) Karst.) stand in southern Sweden. By integrating intra-daily Unmanned Aerial Vehicles (UAV)-based hyperspectral imaging with high-frequency physiological measurements, we aim to establish a mechanistic link between canopy greenness dynamics and hydraulic processes at the crown scale. The performance of the proposed indices is tested against that of the established PRI. Our objectives were:

i. Evaluate whether GSIs derived from high-resolution hyperspectral data can capture the diurnal water use cycle of Norway spruce trees and explore how they relate to hydraulic traits such as leaf water potential and sap flux density derived from hyperspectral data;
ii. Assess the effectiveness of GSIs in capturing daily PAR trajectories (i.e. increase, peak timing, and subsequent decline) and assess the consistency and generalizability of these patterns across the two weeks.

2. Materials and Methods

2.1. Study area and spectral data collection

The study area is a Norway spruce stand located in the Tönnersjöheden Experimental Forest, southern Sweden (Figure 1). The stand has an even-aged and monospecific structure.

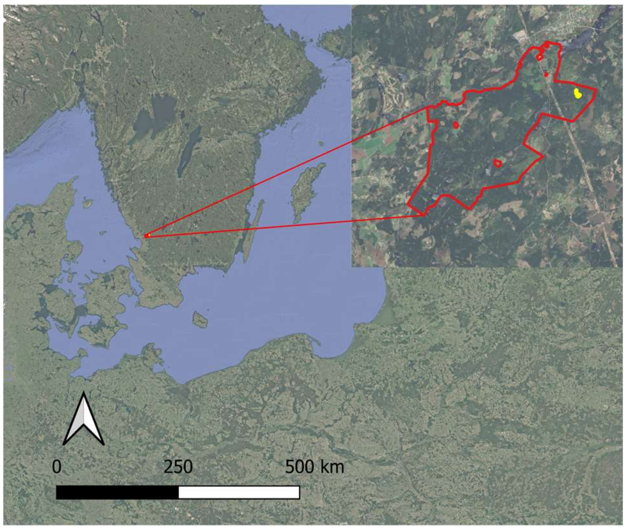

Figure 1: Location and boundaries of the Tönnersjöheden Experimental Forest in southern Sweden. Location of the stand in yellow.

On 2025-08-17 (Week 33 of the year), hyperspectral images were acquired under clear sky conditions using a SPECIM AFX10 sensor (400–1000 nm, 5 nm FWHM) mounted on a FreeFly Alta X drone. Images were acquired again on 2025-09-29 (Week 39), with shorter intervals between flights due to the limitation of shadows caused by lower sun angle. Since there is considerable variability in the interval between the flight times, actual times of the UAV flights and overall length of the interval between first and last flight within the same day in each Week are reported in Table 1.

Week	Approximate flight time	Flight time start (HH:mm)	Flight time end (HH:mm)	Total time interval (hours)
33	9	09:38	09:42	≈ 7
	11	11:08	11:11	
	13	13:56	14:00	
	16	16:39	16:43	
39	11	11:25	11:28	≈ 3
	12	12:11	12:14	
	13	13:20	13:24	
	14	14:20	14:23	

Table 1: Correspondence between approximate and actual UAV flight times and total time interval between the first and last flight in each Week.

Radiometric calibration and geo-rectification of the images were performed in the CaliGeoPRO software (https://www.specim.com/products/caligeo-pro/). Reflectance was estimated using ground targets with near-Lambertian properties placed in the scene for every flight. Small shifts in the processed images were corrected using the Georeferencer tool in QGIS (https://qgis.org/) to match the positions of trees measured in the field using a high-accuracy GNSS system. Crown reflectance was then averaged after performing crown segmentation through a marker-controlled watershed algorithm.

PRI was computed in two different formulations, hereby called $PRI_{530\text{-}570}$ and $PRI_{550\text{-}530}$, according to Equations (Eqs.) 1 (Gamon et al., 1997) and 2 (Peñuelas et al., 1994) respectively:

$$PRI_{530-5} = \frac{R531 - R570}{R531 + R570} \tag{1}$$

$$PRI_{550-530} = \frac{R550 - R531}{R550 + R531} \tag{2}$$

where R is the reflectance at a specific wavelength.

GSCRs were initially derived from inflection and curvature points identified in spectral derivative curves. They were subsequently simplified into combinations of a limited number of bands that capture these spectral features, enabling their application in multispectral data. In this study, we use the simplified multispectral (MS) versions of GSCR1 and GSCR2, following Eqs. 3 and 4 as described in Huo et al. (2024).

$$GSCR1_{MS} = \frac{R550 - R530}{R530 - 0.5 \times (R490 + R550)} \tag{3}$$

$$GSCR2_{MS} = \frac{R550 - R530}{[R530 - 0.5 \times (R490 + R550)] \times (R530 - R490)} \tag{4}$$

A modified formulation of the GSCR1 and GSCR2, more robust against extreme values and hereby called Formulation n.2 (F2), was also tested here (Eqs. 5 and 6),

$$GSCR1_{F2} = \ln\left(\left|\frac{R550 - R530 + \alpha}{R530 - 0.5 \times (R490 + R550) + \alpha}\right|\right) \quad (5)$$

$$GSCR2_{F2} = \ln\left(\left|\frac{(R550 - R530 + \alpha)^2}{[R530 - 0.5 \times (R490 + R550) + \alpha \times (R530 - R490)]}\right|\right) \quad (6)$$

where α = 0.15.

2.2. Environmental and physiological data collection

In 2025, 20 trees were selected and monitored using sapflow sensors throughout the growing season (approximately from middle of June, Week 25, to middle of September, Week 38). Sapflow sensor probes were positioned at 1.3 m of height on each sample tree or moved to a lower position when installation at 1.3 m was not possible. Three probes were inserted at 1, 2 and 3 cm of depth into the bark, and the sap flux density (Js) was measured through the Maximum heat ratio (MHR) method (Lopez et al., 2021) in J/s every 30 minutes and recorded by CR1000 dataloggers and multiplexers (Campbell Scientific Inc.). Js represents the rate at which water moves through the conductive tissue of a tree (Matheny & Bohrer, 2019), and can be used to identify the underlying mechanisms that guide changes in water movement in the plants as well as to examine the responses and functions of vegetation related to water use and environmental changes (Lopez et al., 2021).

In this study, we analyzed how GSIs behave in relation to the outermost (1 cm depth) recorded Js. Upon data quality assessment, we observed that sapflow data from Week 37 onwards were inconsistent due to sensor malfunction; we therefore excluded them from analysis and focused on Js-GSI relationships solely in Week 33. Js records for each tree were normalized at the daily scale to constrain their values between 0 and 1. Records from the same day of the UAV flight (17/08/2025) were matched as closely as possible to the hyperspectral imagery by picking the half-hourly measurements closest to the flight time stamp to ensure direct relation between physiological and spectral information. Consequently, a dataset comprising of 80 Tree-Hour observations was obtained.

Leaf Water Potential (Ψ_{leaf}, MPa) measures the energy status of water in plant leaves, influencing stomatal behavior and transpiration rates (Zhou et al., 2024). Measurements were collected on 24/09/2025 (Week 39) between 10:50 and 14:25 using a Scholander type pressure chamber (PMS Instrument Company, Model 1505D, Albany, OR, USA) on the same 20 sample trees. One south-facing branch per tree was shot from the upper half of the canopy using a shotgun, after which a small twig at the distal end was cut for measurement of $\Psi_{leaf.}$ To account for the effect of time on the measurement, each record was associated only to the closest available flight (i.e. records between 10:50 and 11:45 were associated to spectral data from the 11:00 flight, those between 12:00 and 12:25 to the 12:00 flight, etc.). Figure 2 reports the location of the sample trees considered in the study.

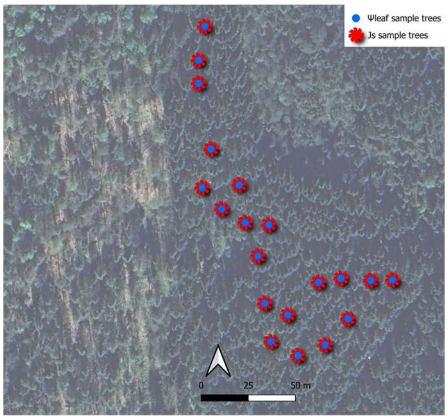

Figure 2: Location of sample trees considered in the study.

The suitability of GSIs to track LUE daily patterns at stand and week scale were analysed using hourly PAR data (W m^{-2}). Data were downloaded via the STRÅNG extraction interface (strang.smhi.se) for days concurrent with the UAV flights (17/08/2025 and 29/09/2925) and interpolated to a 15-minute time step. PAR represents the spectral range of solar radiation (400-700 nm) that vegetation uses in the process of photosynthesis (Azbar & Levin, 2011). The choice of comparing GSI time series to PAR trajectories was made because PAR is a fundamental component of LUE (Fang et al., 2025) which represents the capability of vegetation in utilizing absorbed light for carbon assimilation or biomass accumulation (Sheriff et al., 1995), and as such comparing daily PAR trajectories to GSI time series can offer insights into the suitability of GSIs for tracking photosynthesis dynamics.

Figure 3 presents the time series of the physiological data (Js, Ψ_{leaf}, PAR) plotted against the GSI curves from both Weeks for visual comparison.

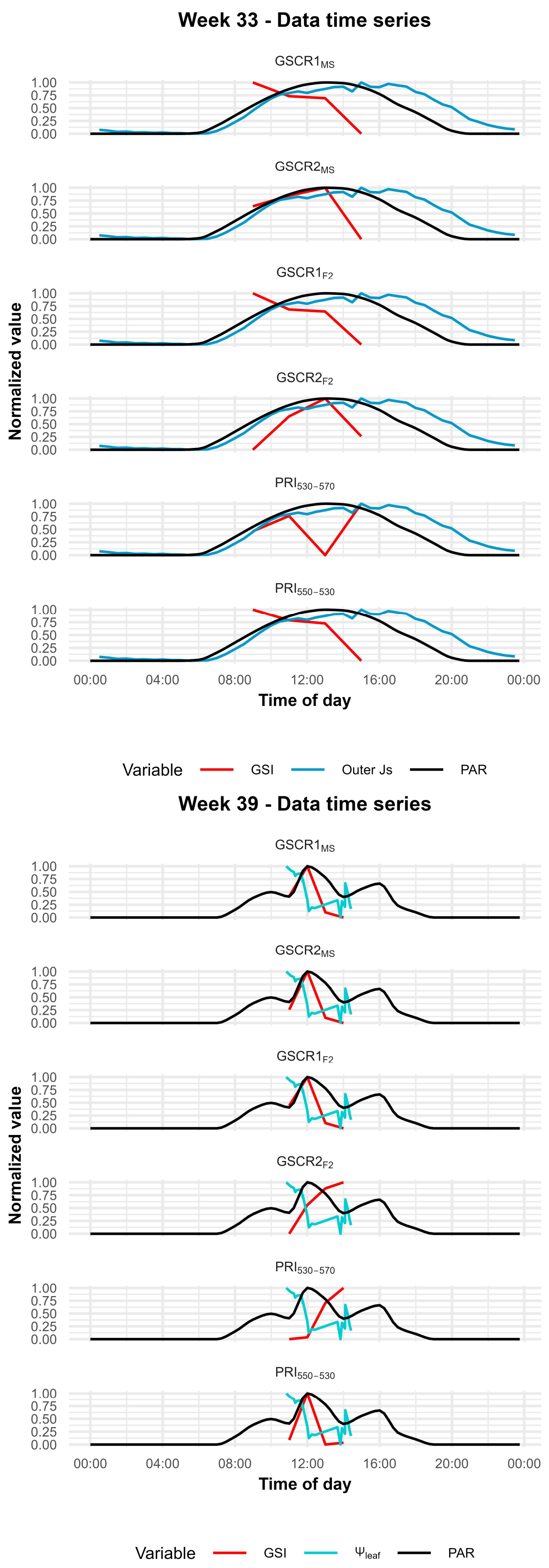

Figure 3: Time series of physiological and spectral data. All time series were normalized between 0 and 1 at daily (Js, PAR) or sub-daily (Ψ_{leaf}, GSI) scale to facilitate visual comparison. Js time series represents an average of all trees in the stand. Top: Week 33 data; bottom: Week 39 data.

2.3. Models and statistical analyses

Logistic regression was applied to evaluate the relationship between Week 33 Js data and GSIs, whereas simple linear models were used to assess the association between GSIs and Week 39 Ψ_{leaf} measurements. Pseudo-R^2 (logistic regression), R^2 (linear regression), p-value and Root Mean Square Error (RMSE) were used to assess the models and compare GSI performance.

The relationship between PAR and the GSI was assessed separately for the two weeks. PAR records were subset based on drone flight times (Table 1) and GSI values from the single sample tree crowns were averaged. Since in this phase we were interested in assessing general stand-level approximation of the PAR curve by GSI records, outliers in the Tree-Hour dataset were removed from the average stand value computation through filtering based on the Interquartile Range (IQR). Both PAR and GSI values were normalized between 0 and 1 within UAV flight intervals to enable direct comparison of their temporal trajectories. The normalization removed differences in magnitude among the different GSIs, allowing us, in this phase, to focus specifically on how accurately the GSI curves approximate PAR dynamics.

The degree of similarity of the GSI curve to PAR trajectory was assessed through means of approximate area between the curves (AABC). The approximate difference between the GSI time series and the corresponding PAR curve was then quantified using the trapezoidal rule (Atkinson, 1989), providing an estimate of the area between the curves over the measurement period. Over the daily measurement period, assuming that the curve between two time steps is roughly linear, the trapezoid area between each time interval was calculated hourly as per Eq. 7

$$A_{tr} = \frac{diff_t - diff_{t+1}}{2} \times \Delta t \tag{7}$$

where $diff_t$ is the difference between the two curves at time t, $diff_{t+1}$ is the difference between the two curves at the next time point, and Δt is the time interval between the two points (in hours). The total difference between the two curves across the entire daily measurement period was then computed according to Eq. 8.

$$AABC = \Sigma A_{tr} \tag{8}$$

3. Results

3.1. Week 33 Js-GSI logistic regression

The results of the logistic regression between Js data and the GSI in Week 33 (Figure 4) revealed significant relationships of Js with GSCR1 (in both formulations) and $PRI_{550-530}$, with a Pseudo-R^2 ranging roughly between 0.2 and 0.3, considerably low p-value ($p < 0.001$) and RMSE within 0.3. Logistic regression failed to converge for the $GSCR2_{MS}$ model due to low variability in the dataset.

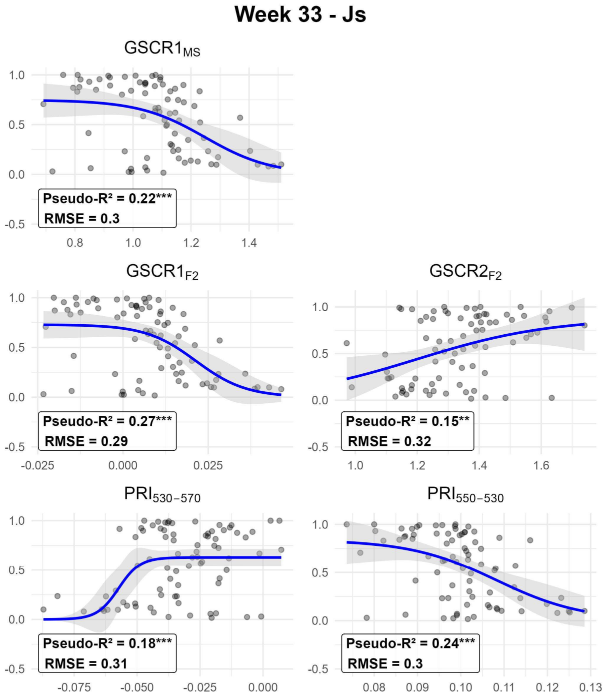

Figure 4: Results of the Js-GSI logistic regression in Week 33. Number of stars indicates p-value significance (* = 0.01-0.05; ** = 0.001-0.01; *** < 0.001).

3.2. Week 39 Ψ_{leaf}-GSI linear regression

Results of the linear regression between the Week 39 Ψ_{leaf} data and GSI are presented in Figure 5. The models revealed no significant relationships with most GSIs, except for a slightly significant one with one of the PRI formulations ($PRI_{550-530}$), an R^2 value of around 0.3 and a RMSE of 0.34.

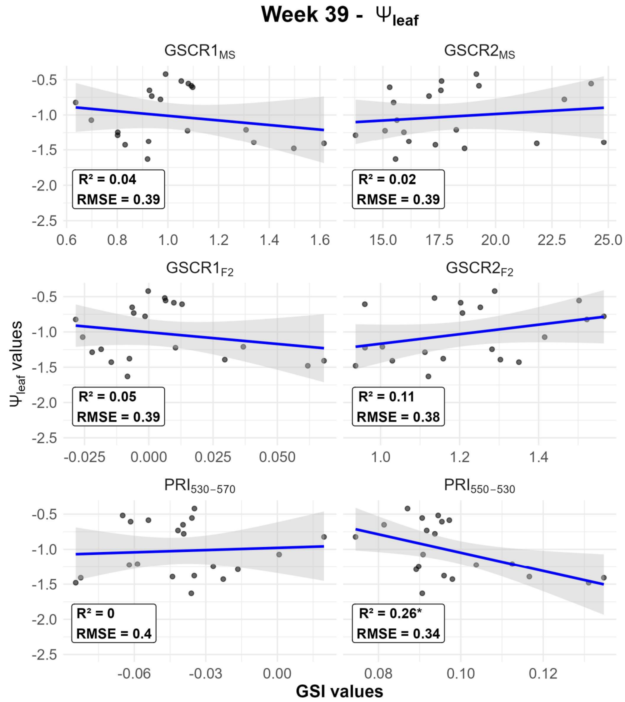

Figure 5: Results of the Ψ_{leaf}-GSI linear regression in Week 39. Number of stars indicates p-value significance (* = 0.01-0.05; ** = 0.001-0.01; *** < 0.001).

3.3. PAR-GSI curve relationships

The normalized PAR and GSI curves for each Week are presented in Figure 6. Daily patterns indicate that GSI temporal dynamics varied significantly between the two weeks. Only $GSCR2_{MS}$ consistently tracked PAR trajectories in both weeks.

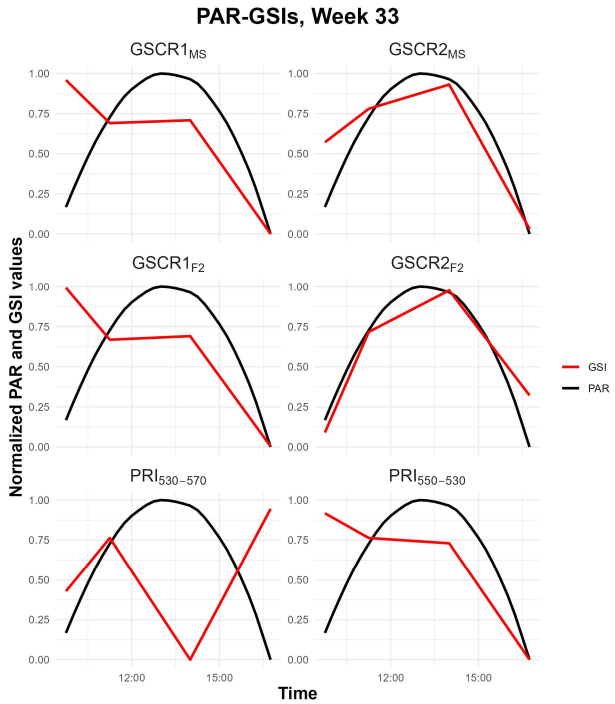

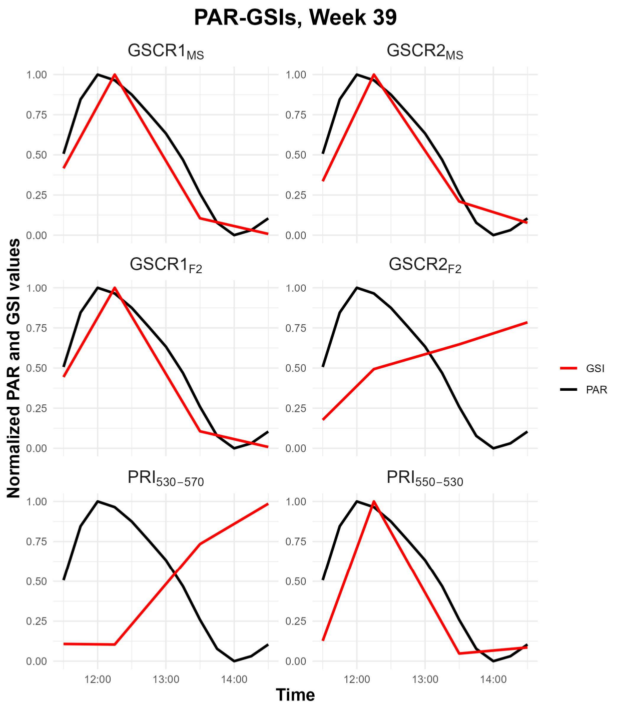

Figure 6: Normalized PAR and GSI curves for Week 33 (top) and Week39 (bottom).

The specific AABCs (Table 3) confirm the findings deduced from the curve plots and reveal that the GSIs that most closely followed the daily PAR dynamics around peak time varied in each Week, with the exception of $GSCR2_{MS}$. GSCR indices generally outperformed PRI, with two (Week 33) and three (Week 39) formulations more closely following PAR dynamics than both PRIs. To allow comparability between the weeks, per-hour AABC was also computed to account for the effect of the different intervals between the first and last UAV flight.

GSI	Week	AABC over the measuring period	AABC per hour
$GSCR1_{MS}$	33	1.38	0.20
$GSCR2_{MS}$		0.55	0.08
$GSCR1_{F2}$		1.50	0.21
$GSCR2_{F2}$		0.56	0.08
$PRI_{530-570}$		4.22	0.60
$PRI_{550-530}$		1.28	0.18
$GSCR1_{MS}$	39	0.29	0.10
$GSCR2_{MS}$		0.17	0.06
$GSCR1_{F2}$		0.28	0.09
$GSCR2_{F2}$		1.37	0.46
$PRI_{530-570}$		1.99	0.66
$PRI_{550-530}$		0.43	0.14

Table 3: Results of the area between curves computation for each Week.

4. Discussion

The results of the Week 33 Js-GSI relationships reveal that logistic regression is suitable to model the response of daily tree hydraulic status using hyperspectral indices. Tree physiological mechanisms rarely follow a linear dynamic, as they involve complex interactions and interconnected processes (e.g. Li et al., 2022; Nasiri et al., 2025; Osland et al., 2015), and the simple linear function that we fitted precedingly and for the sake of brevity didn’t report here didn’t capture as much variability in our dataset as the logistic regression we later chose to employ, which is better suited to follow daily Js dynamics through the monitoring of changes in crown reflectance, as suggested by previous studies where the relationship between sapflow data and other environmental variables were investigated (e.g. Gimenez et al., 2019; O’Brien et al., 2004).

The two GSCR1 formulations (Figure 4) capture a satisfactory level of variability in the Js dataset, with moderate decrease within certain GSI value ranges, preceded a plateau, suggesting a decoupling between canopy greenness or photosynthetic activity and Js, possibly due to the involvement of regulatory mechanisms of photoprotection (Niyogi, 1999) or cooling (Krich et al., 2022). $PRI_{550-530}$ also follows a similar trend. While the Pseudo-R^2 values, roughly between 0.2 and 0.3, are not considerably high, they are deemed acceptable in experimental designs involving open-environment measurements such as the one we conducted here, where there is a strong effect of external factors such as soil characteristics, moisture, or single tree differences (Lin & Wiegand, 2023). Furthermore, the goodness of these models is proved by their significant p-value and acceptable RMSE (within the limit of 0.3) for evaluation of trends in a dataset acquired within open-environment conditions.

Moving to Week 39 Ψ_{leaf} (Figure 5), the results of the linear regression appear mostly insignificant, save for the $PRI_{550-530}$ model, which, however, has higher than acceptable RMSE (> 0.3), pointing to the fact that the index poorly captures the underlying trend in the Ψ_{leaf} data. This can be attributed to several factors, such as the small number of observations (20 in total, collected in a single day), lower temporal coupling accuracy with the GSI dataset and larger error possibility due to human handling of the samples. However, the Ψ_{leaf}-GSI relationships noticeably show similar patterns to the Js-GSI ones, with similar trends, suggesting that similar ecophysiological mechanisms could be at play. It is therefore possible that, if a larger number of observations were available, more solid conclusions could be drawn regarding the Ψ_{leaf}-GSI relationship. This will be explored further in subsequent work, as more Ψ_{leaf} measures are going to be collected in the stand presented here as well as in another experimental site within the Tönnersjöheden forest.

The analysis of the relationship between PAR curves and GSI time series (Figure 6) indicates that no robust, generalizable pattern exists across both weeks, with the exception of $GSCR2_{MS}$, which consistently mirrors PAR. However, GSCR indices generally outperform PRI, with at least two (Week 33, Figure 6 – top) or three (Week 39, Figure 6 – bottom) indices capturing the increase, peak, and decline of the PAR trajectory, as further supported by the AABC results (Table 3). This supports what was already suggested by Huo et al. (2024) regarding the greater potential of GSCR indices in capturing the photochemical functioning of vegetation.

Overall, the PAR-GSI time series relationships appear to be week-specific. It is possible that at different times of the year, different GSI may be more appropriate in tracking photosynthetic dynamics in Norway spruce, due to shifts in pigment concentrations (Hejtmánek et al., 2022). In this sense, confronting GSI curves with photosynthesis-related physiological mechanisms, such as LUE and Sun-Induced Fluorescence (SIF) measurements, might reveal additional underlying patterns in the suitability of GSI when tracking these dynamics. Additionally, the circumstances of image acquisition (e.g. differences in illumination, sun-sensor geometry, and imaging intervals between two separate times of the year) could contribute to variability in the digital number values recorded by the hyperspectral sensor, highlighting an additional source of uncertainty to be addressed in future research. Ultimately, additional studies at this stand, as well as at another site within the Tönnersjöheden experimental forest, will further investigate and clarify the drivers underlying differential GSI trajectories. Such work will also incorporate comparisons with the additional site within the experimental forest and address sources of uncertainty and differential behaviors, not presented here for the sake of brevity.

5. Conclusions

In this study, we compared the performance of six GSIs in tracking daily hydraulic status dynamics in a Norway spruce stand. We achieved this by comparing intra-daily drone acquisitions in two different times of the year with daily, single-tree Js and Ψ_{leaf} measures as well as with PAR curves as a driver of LUE.

Overall, GSIs proved effective in tracking daily variations in tree hydraulic status through changes in crown reflectance. Among the tested indices, the two GSCR1 formulations consistently showed a significant relationship with Js measures, generally outperforming the commonly employed PRI. In contrast, Ψ_{leaf} measurements were less conclusive: although they exhibited trends broadly consistent with Js-GSI relationships, their more limited temporal resolution and potential mismatches between measurement and flight timing likely reduced their explanatory power. With improved temporal alignment and a larger dataset, Ψ_{leaf} could provide more robust insights into their daily dynamics. No clear relationships emerged between PAR and GSI trajectories save for one GSI ($GSCR2_{MS}$), suggesting that shifts in greenness due to different times of the year, as well as imagery acquisition circumstances, might be affecting these interactions. This highlights the complexity of linking spectral indices directly to radiation-driven physiological processes under field conditions.

Overall, our findings demonstrate the potential of high-resolution hyperspectral imaging for monitoring tree hydraulic processes at fine temporal scales. However, some of the contrasting responses observed between the two weeks regarding the PAR-GSI relationship underscore the importance of accounting for specific conditions, as assessing relationships between physiological and spectral data at different times of the year, even on the same site, can lead to divergent responses. Furthermore, caution should be given to the imagery acquisition phase, as subtle differences in flight timing, illumination and sun-sensor geometry can significantly influence spectral values. Future work will focus on expanding the dataset and refining acquisition protocols to improve characterization of GSI behavior in relation to ecophysiological processes, and to better disentangle the environmental drivers underlying week-specific dynamics. Incorporating data from an additional stand within the site, along with a systematic assessment of the factors driving divergent trajectories, will further clarify the relationships between tree physiological variables and GSI. This will also enable a more robust evaluation of the GSI's suitability for tracking vegetation dynamics across stands and throughout different periods of the year.

Acknowledgements

This research project is funded by the Forest Damage Centre at the Swedish University of Agricultural Sciences [project grants SLU.sfak.2022.1.1.1-304-5, SLU.sfak.2023.1.1.1-115-12, SLU.sfak 2025-234-07, SLU.sfak.2025.1.1-293-11 to LH, sfak 2023-376-11 to LS], the Swedish Research Council for Sustainable Development Formas [project grant 2024-00404 to LH and 2024-00286 to LS], the Kempestiftelserna [project grants JCSMK22-0126, JCSMK23-0096, and JCSMK25-0054 to LH], and Carl Tryggers Foundation for Scientific Research [project grant CTS 24:3661 to LH].

The authors acknowledge Dr. Martin Goude's support in the development of this study. Dr. Goude and the team at Tönnersjöheden Experimental Forest provided the facilities and logistical support necessary for this research.

The authors acknowledge Associate Professor Maartje Klapwijk for providing access to the experimental site.

References

Atkinson, K. E. (1989.). *An Introduction to Numerical Analysis, 2nd Edition.* Wiley. ISBN: 978-0-471-62489-9

Azbar, N., & Levin, D. B. (2011). In *Biohydrogen Production from Agricultural Agrofood-Based Resources* (Vol. 6, pp. 629–641). Academic Press. https://doi.org/10.1016/B978-0-08-088504-9.00391-3

D'Odorico, P., Schönbeck, L., Vitali, V., Meusburger, K., Schaub, M., Ginzler, C., Zweifel, R., Velasco, V. M. E., Gisler, J., Gessler, A., & Ensminger, I. (2021). Drone-based physiological index reveals long-term acclimation and drought stress responses in trees. *Plant, Cell & Environment*, *44*(11), 3552–3570. https://doi.org/10.1111/pce.14177

Demmig-Adams, B., & Adams, W. W. (1996). The role of xanthophyll cycle carotenoids in the protection of photosynthesis. *Trends in Plant Science*, *1*(1), 21–26. https://doi.org/10.1016/S1360-1385(96)80019-7

Fang, J., Lian, X., Ryu, Y., Jeong, S., Jiang, C., & Gentine, P. (2025). A long-term reconstruction of a global photosynthesis proxy over 1982–2023. *Scientific Data*, *12*(1), 372. https://doi.org/10.1038/s41597-025-04686-6

Gamon, J. A., Serrano, L., & Surfus, J. S. (1997). The photochemical reflectance index: An optical indicator of photosynthetic radiation use efficiency across species, functional types, and nutrient levels. *Oecologia*, *112*(4), 492–501. https://doi.org/10.1007/s004420050337

Gimenez, B. O., Jardine, K. J., Higuchi, N., Negrón-Juárez, R. I., Sampaio-Filho, I. de J., Cobello, L. O., Fontes, C. G., Dawson, T. E., Varadharajan, C., Christianson, D. S., Spanner, G. C., Araújo, A. C., Warren, J. M., Newman, B. D., Holm, J. A., Koven, C. D., McDowell, N. G., & Chambers, J. Q. (2019). Species-

Specific Shifts in Diurnal Sap Velocity Dynamics and Hysteretic Behavior of Ecophysiological Variables During the 2015–2016 El Niño Event in the Amazon Forest. *Frontiers in Plant Science*, *10*. https://doi.org/10.3389/fpls.2019.00830

Gitelson, A. A., Gamon, J. A., & Solovchenko, A. (2017). Multiple drivers of seasonal change in PRI: Implications for photosynthesis 2. Stand level. *Remote Sensing of Environment*, *190*, 198–206. https://doi.org/10.1016/j.rse.2016.12.015

Hejtmánek, J., Stejskal, J., Čepl, J., Lhotáková, Z., Korecký, J., Krejzková, A., Dvořák, J., & Gezan, S. A. (2022). Revealing the Complex Relationship Among Hyperspectral Reflectance, Photosynthetic Pigments, and Growth in Norway Spruce Ecotypes. *Frontiers in Plant Science*, *13*. https://doi.org/10.3389/fpls.2022.721064

Huo, L., Koivumäki, N., Oliveira, R. A., Hakala, T., Markelin, L., Näsi, R., Suomalainen, J., Polvivaara, A., Junttila, S., & Honkavaara, E. (2024). Bark beetle pre-emergence detection using multi-temporal hyperspectral drone images: Green shoulder indices can indicate subtle tree vitality decline. *ISPRS Journal of Photogrammetry and Remote Sensing*, *216*, 200–216. https://doi.org/10.1016/j.isprsjprs.2024.07.027

Inoue, Y., & Peñuelas, J. (2006). Relationship between light use efficiency and photochemical reflectance index in soybean leaves as affected by soil water content. *International Journal of Remote Sensing*, *27*(22), 5109–5114. https://doi.org/10.1080/01431160500373039

Krich, C., Mahecha, M. D., Migliavacca, M., De Kauwe, M. G., Griebel, A., Runge, J., & Miralles, D. G. (2022). Decoupling between ecosystem photosynthesis and transpiration: A last resort against overheating. *Environmental Research Letters*, *17*(4), 044013. https://doi.org/10.1088/1748-9326/ac583e

Li, X., Xi, B., Wu, X., Choat, B., Feng, J., Jiang, M., & Tissue, D. (2022). Unlocking Drought-Induced Tree Mortality: Physiological Mechanisms to Modeling. *Frontiers in Plant Science*, *13*. https://doi.org/10.3389/fpls.2022.835921

Lin, S., Lai, J., Yin, G., Fang, J., Liu, X., Zhang, X., Yang, H., Yang, P., & Xiao, Q. (2026). Linking the diurnal and seasonal dynamic of photochemical reflectance index and photosynthesis in a paddy rice field. *Smart Agricultural Technology*, *13*, 101775. https://doi.org/10.1016/j.atech.2025.101775

Lin, Y., & Wiegand, K. (2023). Low R2 in ecology: Bitter, or B-side? *Ecological Indicators*, *153*, 110406. https://doi.org/10.1016/j.ecolind.2023.110406

Lopez, J. G., Pypker, T., Licata, J., Burgess, S. S. O., & Asbjornsen, H. (2021). Maximum heat ratio: Bi-directional method for fast and slow sap flow measurements. *Plant and Soil*, *469*(1), 503–523. https://doi.org/10.1007/s11104-021-05066-w

Matheny, A. M., & Bohrer, G. (2019). *3.7 Sap flux*. ClimEx Handbook. https://climexhandbook.w.uib.no/2019/11/05/sap-flux/

Möttus, M., Hernández-Clemente, R., Perheentupa, V., Markiet, V., Aalto, J., Bäck, J., & Nichol, C. J. (2018). Measurement of Diurnal Variation in Needle PRI and Shoot Photosynthesis in a Boreal Forest. *Remote Sensing*, *10*(7), 1019. https://doi.org/10.3390/rs10071019

Nasiri, V., Hawryło, P., Tymińska-Czabańska, L., & Socha, J. (2025). Not always in sync: Environmental drivers of the relationship between tree radial growth and vegetation indices in Central Europe. *Science of The Total Environment*, *1008*, 180969. https://doi.org/10.1016/j.scitotenv.2025.180969

Niyogi, K. K. (1999). PHOTOPROTECTION REVISITED: Genetic and Molecular Approaches. Annual Review of Plant Physiology and Plant Molecular *Biology*, 50, 333–359. https://doi.org/10.1146/annurev.arplant.50.1.333

O'Brien, J. J., Oberbauer, S. F., & Clark, D. B. (2004). Whole tree xylem sap flow responses to multiple environmental variables in a wet tropical forest. *Plant, Cell & Environment*, *27*(5), 551–567. https://doi.org/10.1111/j.1365-3040.2003.01160.x

Osland, M. J., Day, R. H., From, A. S., McCoy, M. L., McLeod, J. L., & Kelleway, J. J. (2015). Life stage influences the resistance and resilience of black mangrove forests to winter climate extremes. *Ecosphere*, *6*(9), art160. https://doi.org/10.1890/ES15-00042.1

Peñuelas, J., Gamon, J. A., Fredeen, A. L., Merino, J., & Field, C. B. (1994). Reflectance indices associated with physiological changes in nitrogen- and water-limited sunflower leaves. *Remote Sensing of Environment*, *48*(2), 135–146. https://doi.org/10.1016/0034-4257(94)90136-8

Sheriff, D. W., Margolis, H. A., Kaufmann, M. R., & Reich, P. B. (1995). Resource Use Efficiency. In *Resource Physiology of Conifers* (pp. 143–178). Academic Press. https://doi.org/10.1016/B978-0-08-092591-2.50010-8

Zhou, S., Zhou, J., Pan, Y., Wu, Q., & Ping, J. (2024). Wearable electrochemical sensors for plant small-molecule detection. *Trends in Plant Science, Special Issue: 21st Century Tools in Plant Science*, *29*(2), 219–231. https://doi.org/10.1016/j.tplants.2023.11.013